Cross-polarization error correction enhanced polarization-division-multiplexed differential detection system for optical fiber communications

Chenxu Jiang
Suzhou Key Laboratory of Advanced Optical Communication Network Technology
Soochow University
Suzhou, China

Yi Cai *
Suzhou Key Laboratory of Advanced Optical Communication Network Technology
Soochow University
Suzhou, China
* yicai@suda.edu.cn

Xiaozhou Wang
Jiangsu Hengxin Semitech Co., Ltd
Suzhou, China

Zhongxing Tian
Suzhou Key Laboratory of Advanced Optical Communication Network Technology
Soochow University
Suzhou, China

Fuhan Wang
Jiangsu Hengtong Optic-electric Co., Ltd
Suzhou, China

Huan Huang
Suzhou Key Laboratory of Advanced Optical Communication Network Technology
Soochow University
Suzhou, China

Jun Zhou
Jiangsu Hengxin Semitech Co., Ltd
Suzhou, China

Xiangyong Hao
Jiangsu Hengtong Optic-electric Co., Ltd
Suzhou, China

Shengqing Pang
Jiangsu Hengtong Optic-electric Co., Ltd
Suzhou, China

***Abstract*—We propose a novel cross-polarization error correction (CPEC) algorithm for polarization-division-multiplexed differential quadrature-phase-shift-keying (PDM-DQPSK) systems. The obtained results show that 1-dB sensitivity improvement can be achieved at 1×10^{-3} forward-error-correction (FEC) threshold.**

Keywords—polarization division multiplexing, differential quadrature-phase-shift-keying, error detection and correction, coherent optical communication, digital signal processing

I. INTRODUCTION

With the advancement of cloud computing, the Internet of Things (IoT), and 5G technologies, global network traffic is rapidly growing. Currently, conventional low-cost short-reach optical fiber communication systems utilize intensity modulation direct detection (IMDD) schemes [1] and have limited data rates due to low receiver sensitivity and spectral efficiency (SE). A more efficient detection scheme is needed to enhance the transmission system performance, such as polarization division multiplexing (PDM) coherent detection. However, implementing coherent detection in short-reach systems faces the challenge of requiring a narrow linewidth laser as local oscillator (LO) [2].

In order to address this challenge, a self-homodyne coherent detection (SHCD) scheme has been proposed in recent years [3-6]. In this scheme, a laser source at the transmitter is divided into two parts. One serves as signal carrier and the other is transmitted without modulation as a remote LO for the receiver. This scheme reduces the impact of phase noise from the laser, allowing for a larger linewidth laser to lower costs. However, the state of polarization of the remotely delivered LO is unstable, therefore, an active polarization controller (APC) in the optical domain is required. Currently, maximum tracking speed of the APC for SHCD systems is around 200krad/s [7], raising a challenge for further improvement in the optical domain. A complementary polarization-diversity coherent receiver (C-PDCR) has been proposed [8, 9] that incorporates a third complementary hybrid for the remixture of the LO and signal to meet this challenge. This design allows for higher polarization tracking speed with the help of digital signal processing (DSP) techniques.

An alternative to the SHCD scheme is a polarization-division-multiplexed differential quadrature-phase-shift-keying (PDM-DQPSK) scheme for LO-less differential self-coherent detection (DSCD) [10]. This scheme utilizes an extra set of 90-degree hybrids and balanced detectors (BDs) to generate cross-polarization beating terms, enabling faster polarization tracking and comparable sensitivity to the SHCD system. Nevertheless, the cross-polarization beating terms generated by the scheme are only utilized for digital polarization demultiplexing and are not recognized as a potential resource to improve receiver sensitivity. After demultiplexing, the cross-polarization terms are considered worthless and discarded rather than being utilized to further improve receiver performance.

Hence, in this study, we propose a novel cross-polarization error correction (CPEC) algorithm that significantly improves receiver performance of a differential self-coherent PDM-DQPSK system. The algorithm utilizes the relationship between the co- and cross-polarization terms to detect and correct errors. A LO-less differential self-coherent optical receiver and digital domain polarization demultiplexing are employed, and the cross-polarization terms are fully utilized to enhance the receiver sensitivity. Our simulations show that the CPEC-enhanced DSCD based PDM-DQPSK system outperforms both the SHCD based PDM-QPSK system and the C-PDCR based PDM-QPSK system with better bit error

This work was supported by the National Key R&D Program of China (2022YFB2903000) and the National Natural Science Foundation of China (62275185, 62250710164).

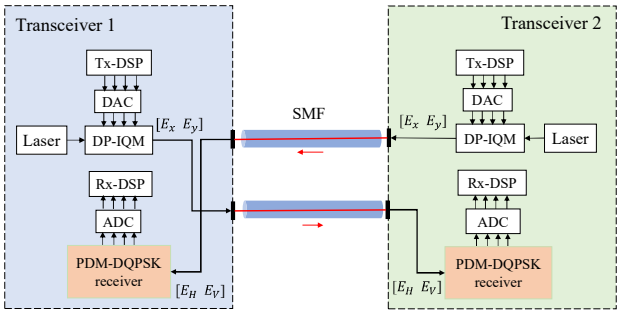

Fig. 1. Schematic of a differential self-coherent PDM-DQPSK system

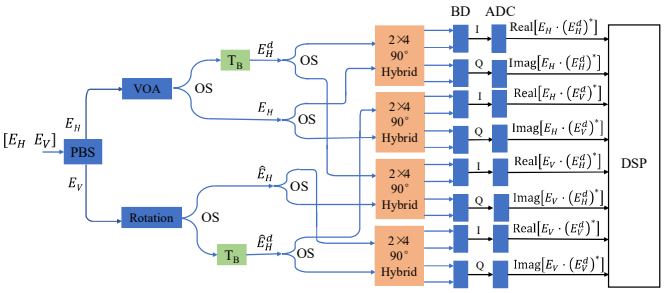

Fig. 2. LO-less differential self-coherent PDM-DQPSK receiver front-end structure. PBS: polarization beam splitter, VOA: variable optical attenuator, OS: optical splitter, BD: balanced detector, DSP: digital signal processing

rate (BER) vs. optical signal to noise ratio (OSNR) performance and higher laser linewidth tolerance.

In this paper, x^T denotes the transposition of the quantity x, x^* is the complex conjugate of the quantity x, and x^d represents a delay of one symbol period for the quantity x. The decision bits corresponding to the k-th phase X_k are denoted as X_k^b. $X_I^b(k)$ and $X_Q^b(k)$ refer to the in-phase and quadrature bit of X_k^b.

II. Principle of the CPEC-enhanced Differential Self-Coherent PDM-DQPSK System

A. Structure of Differential Self-Coherent System

Fig. 1 schematically shows a differential self-coherent PDM-DQPSK system including two transceivers. The output of a digital-to-analog converter (DAC) in the transceiver drives the DP-IQM, and a laser is used for modulation. The modulated signal is then transmitted from transceiver 1 to transceiver 2 through fiber.

Assuming that PDM-DQPSK signal is expressed as $[E_x \quad E_y]^{\mathrm{T}}$, the polarization rotation matrix $\mathbf{R}$ is expressed as

$$\mathbf{R} = \begin{bmatrix} \cos\theta & -\sin\theta\, e^{j\varphi} \\ \sin\theta\, e^{-j\varphi} & \cos\theta \end{bmatrix}, \tag{1}$$

where θ is the azimuth angle, φ is the angle of elevation.

Thus, the received signal can be expressed as

$$\begin{bmatrix} E_H \\ E_V \end{bmatrix} = \mathbf{R} \begin{bmatrix} E_x \\ E_y \end{bmatrix}. \tag{2}$$

Transceiver 2 employs a LO-less front-end design [10], as illustrated in Fig. 2. The receiver creates cross-polarization beating between the two orthogonal signal polarizations by incorporating an additional set of 90-degree hybrids and BDs.

The received dual-polarization signal is split by a polarization beam splitter (PBS) into two orthogonal components, E_H and E_V. A variable optical attenuator (VOA) is added to balance the power between the two polarizations. To induce beating between the two polarizations, E_V is rotated to the same mode as E_H, labeled as $\hat{E}_H$, and after delaying one symbol period T_B for both E_H and $\hat{E}_H$, an extra delayed copy of E_H, denoted as E_H^d, and an extra delayed copy of $\hat{E}_H$, denoted as $\hat{E}_H^d$, are obtained. Through the use of hybrids and BDs, the co-polarization beating ($E_H \cdot (E_H^d)^*$ and $E_V \cdot (E_V^d)^*$) and cross-polarization beating ($E_H \cdot (E_V^d)^*$ and $E_V \cdot (E_H^d)^*$) can be derived. The outputs of the analog-to-digital converter (ADC) of the co- and cross-polarization beating terms are processed by the Rx-DSP.

The co- and cross-polarization beating terms generated by the differential self-coherent receiver are described in (3)-(6), as shown at the bottom of the page. The symbol S represents $[E_x(E_x^d)^* \quad E_x(E_y^d)^* \quad E_y(E_x^d)^* \quad E_y(E_y^d)^*]$. The terms $E_x(E_x^d)^*$ and $E_y(E_y^d)^*$ denote the co-polarization differential phases, while $E_x(E_y^d)^*$ and $E_y(E_x^d)^*$ represent the cross-polarization differential phases.

Combining the co-polarization and cross-polarization beating terms, we obtain matrix $\mathbf{M}$ shown in (7) at the bottom of the page. This allows us to express the co- and cross-polarization beating terms as

$$\begin{bmatrix} E_H \cdot (E_H^d)^* \\ E_H \cdot (E_V^d)^* \\ E_V \cdot (E_H^d)^* \\ E_V \cdot (E_V^d)^* \end{bmatrix} = \mathbf{M} \begin{bmatrix} E_x(E_x^d)^* \\ E_x(E_y^d)^* \\ E_y(E_x^d)^* \\ E_y(E_y^d)^* \end{bmatrix}. \tag{8}$$

By introducing the cross-polarization beating terms, the 2×2 polarization rotation matrix $\mathbf{R}$ is expanded to a 4×4 matrix, denoted as $\mathbf{M}$. $\mathbf{M}$ is a non-singular matrix, meaning that it has an inverse matrix, denoted as $\mathbf{M}^{-1}$. With the 4x4 multi-input-multi-output (MIMO) adaptive equalization algorithm, the received dual-polarization signal can be accurately tracked, demultiplexed, and equalized.

$$E_H \cdot (E_H^d)^* = [\cos^2\theta \quad -\cos\theta \cdot \sin\theta e^{-j\varphi} \quad -\sin\theta e^{j\varphi} \cdot \cos\theta \quad \sin^2\theta] S^T \tag{3}$$

$$E_V \cdot (E_V^d)^* = [\sin^2\theta \quad \sin\theta e^{-j\varphi} \cdot \cos\theta \quad \cos\theta \cdot \sin\theta e^{j\varphi} \quad \cos^2\theta] S^T \tag{4}$$

$$E_H \cdot (E_V^d)^* = [\cos\theta \cdot \sin\theta e^{j\varphi} \quad \cos^2\theta \quad -\sin^2\theta e^{j2\varphi} \quad -\sin\theta e^{j\varphi} \cdot \cos\theta] S^T \tag{5}$$

$$E_V \cdot (E_H^d)^* = [\sin\theta e^{-j\varphi} \cdot \cos\theta \quad -\sin^2\theta e^{-j2\varphi} \quad \cos^2\theta \quad -\cos\theta \cdot \sin\theta e^{-j\varphi}] S^T \tag{6}$$

$$\mathbf{M} = \begin{bmatrix} \cos^2\theta & -\cos\theta \cdot \sin\theta e^{-j\varphi} & -\sin\theta e^{j\varphi} \cdot \cos\theta & \sin^2\theta \\ \cos\theta \cdot \sin\theta e^{j\varphi} & \cos^2\theta & -\sin^2\theta e^{j2\varphi} & -\sin\theta e^{j\varphi} \cdot \cos\theta \\ \sin\theta e^{-j\varphi} \cdot \cos\theta & -\sin^2\theta e^{-j2\varphi} & \cos^2\theta & -\cos\theta \cdot \sin\theta e^{-j\varphi} \\ \sin^2\theta & \sin\theta e^{-j\varphi} \cdot \cos\theta & \cos\theta \cdot \sin\theta e^{j\varphi} & \cos^2\theta \end{bmatrix} \tag{7}$$

B. Principle of Cross Polarization Error Correction

In this section, we describe the error detection and correction scheme using relationship between the co-polarization and cross-polarization differential phases, and then correct errors with the help of the cross-polarization terms to improve performance of the differential self-coherent PDM-DQPSK system.

After 4×4 MIMO adaptive equalization, the co-polarization differential phases and the cross-polarization differential phases are obtained simultaneously, which are correlated, allowing for the detection and correction of errors that occurred during the differential detection process.

The absolute phase of the k-th symbol in polarization X and Y is represented by X_k and Y_k, respectively. The co-polarization differential phases between two consecutive symbols in the same polarization, generated by $E_x(E_x^d)^*$ and $E_y(E_y^d)^*$ can be expressed as

$$\Delta x_k = X_{k+1} - X_k,\ \Delta y_k = Y_{k+1} - Y_k, \tag{9}$$

and the cross-polarization differential phases generated by $E_x(E_y^d)^*$ and $E_y(E_x^d)^*$ can be expressed as

$$\Delta h_k = X_{k+1} - Y_k,\ \Delta v_k = Y_{k+1} - X_k. \tag{10}$$

By utilizing (9) and (10), a constraint relationship can be derived

$$\Delta h_k + \Delta v_k = \Delta x_k + \Delta y_k. \tag{11}$$

In the differential self-coherent PDM-DQPSK system, both the co-polarization differential phases (Δx and Δy) and the cross-polarization differential phases (Δh and Δv) contain the same transmitted bits. This means that the transmitted bits can be recovered using either the co-polarization differential phases or the cross-polarization differential phases. Additionally, the constraint relationship between these differential phases can be used to identify potential errors in transmission. If $\Delta x + \Delta y = \Delta h + \Delta v$, there is no detectable error. Otherwise, there might be an error occurrence.

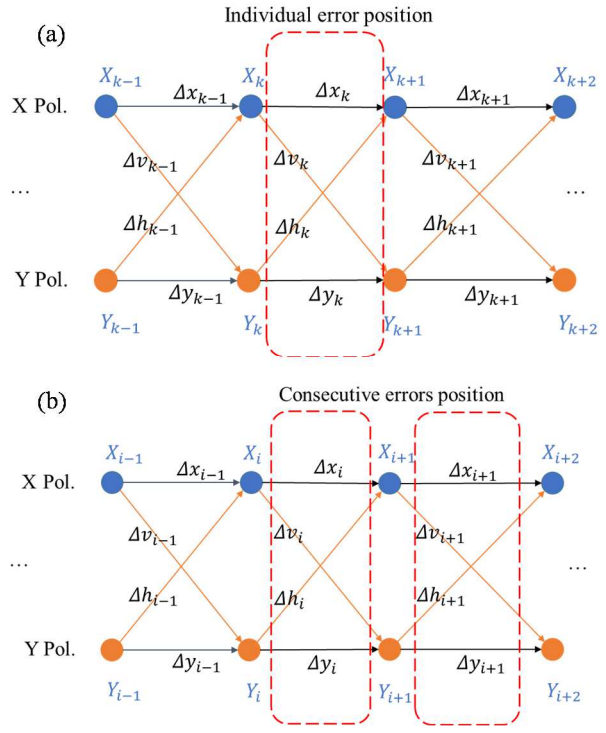

Fig. 3. Different categories of errors observed in the CPEC process: (a) individual error, (b) consecutive errors

The CPEC algorithm classifies detectable errors into two categories: individual error and consecutive errors, as shown in Fig. 3(a) and (b). The simulations demonstrate that the majority of symbol errors detected through the constraint relationship appear individually as shown in Fig. 4. The consecutive errors account for around 1/4 of the total errors when OSNR is 16 dB and much less when the OSNR is higher. This shows a low consecutive error probability where two adjacent symbols are both incorrect in the received sequence, making it easier to focus on isolated individual symbol error during the CPEC process. At each position, there are four differential phases. As depicted in Fig. 3(a), solid lines represent the differential phases and solid circles represent the absolute phases. In this paper, the CPEC algorithm obtains potential error locations from the constraint relationship, disregards consecutive-error cases and only focuses on individual-error cases, the application of which employs only hard decision to keep the complexity low.

The phases pi, $pi/2$, $(3 * pi)/2$, and 0 correspond to symbols 00, 01, 10, and 11, respectively. By analyzing the relationship between the phases, the logical relationships shown in Tables 1 and 2 can be derived. As a result, the phase operation can be replaced by a logical operation. Thus, X_{k+1}^b can be obtained from X_k^b and Δx_k^b as shown in Table 1, or from Y_k^b and Δh_k^b as shown in Table 2. The relationship between Y_k^b, Y_{k+1}^b and Δy_k^b is similar to Table 1, while the relationship between X_k^b, Y_{k+1}^b and Δv_k^b is similar to Table 2.

After the received differential phase is converted to bits, as shown in Fig. 3(a) and Fig. 5, the proposed CPEC algorithm is executed as follows:

1) Obtaining the locations of potential error from the differential phase constraint relationship.

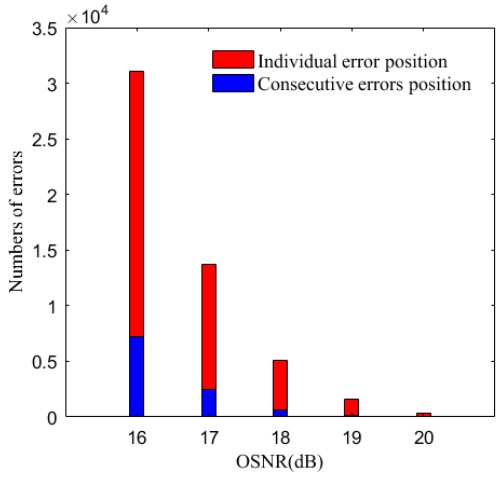

Fig. 4. numbers of individual and consecutive symbol errors in the received sequence at different OSNR for the differential self-coherent PDM-DQPSK system

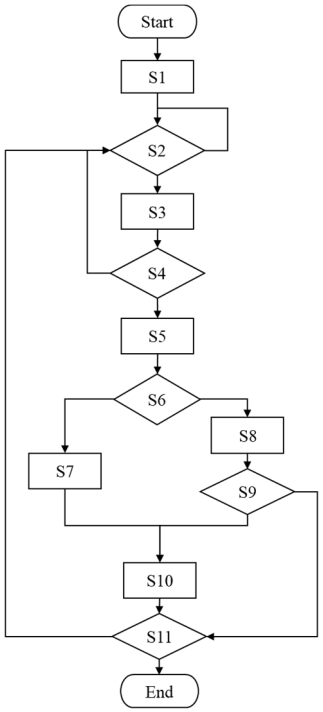

Fig. 5. Flow chart of the CPEC algorithm

2) Performing the next step for an individual-error position, skipping consecutive-error positions to the next position and performing step S2 again.

3) Utilizing the co- and cross-polarization terms, the correct absolute terms can be obtained. The correct X_{k-1}^b, X_k^b, Y_{k-1}^b, and Y_k^b are determined using the co- and cross-polarization terms at the (k-1)th correct position, the detailed step is as follows:

a) The initial values of X_{k-1}^b and Y_{k-1}^b are assigned, X_k^b and Y_k^b are calculated using the co-polarization differential terms Δx_{k-1}^b and Δy_{k-1}^b, and the cross-polarization differential terms Δh_{k-1}^b and Δv_{k-1}^b from Tables 1 and 2.

b) Then, the results obtained from the co- and cross-polarization terms are compared. If they are the same, X_k^b and Y_k^b can be determined. Otherwise, by repeating the possible assignment combination of X_{k-1}^b and Y_{k-1}^b, comparing X_k^b and Y_k^b from the co- and cross-polarization terms, a more reliable estimation of the absolute values of symbols X_k^b and Y_k^b can be obtained.

4) If X_k^b and Y_k^b are determined at step S3, then continue to the next step. Otherwise, the algorithm fails to correct this error, returns to S2 and carries out the next position.

5) Next, we obtain four absolute terms from the differential terms at the error position k. The (k+1)th group absolute terms from the co-polarization and cross-polarization terms are compared.

6) If the absolute terms from the co- and cross-polarization terms are equal, we can determine either X_{k+1}^b or Y_{k+1}^b, goto step S7, otherwise goto step S8.

7) If the X_{k+1}^b is determined, the value of Y_{k+2}^b can be calculated using the correct Δv_{k+1}^b and X_{k+1}^b. The other symbol Y_{k+1}^b is calculated from Δy_{k+1}^b and Y_{k+2}^b. If the Y_{k+1}^b is determined, the process is similar. So we can obtain both X_{k+1}^b and Y_{k+1}^b.

8) X_{k+1}^b, X_{k+2}^b, Y_{k+1}^b, and Y_{k+2}^b can be calculated using the differential terms at the (k +1)th correct position, following a similar process as step S3.

9) If the absolute symbols of the (k+2)th group are obtained in step S8, the algorithm goes to step S10 for error correction. Otherwise, it goes to step S11 for the next position.

10) Error is corrected using X_k^b, X_{k+1}^b, Y_k^b, *and* Y_{k+1}^b.

11) If the processed position is the last wrong position, the error correction algorithm is terminated. Otherwise, it goes to step S2 to process the next position.

TABLE 1. RELATIONSHIP BETWEEN TRANSMITTED BITS AND CO-POLARIZATION DECISION BITS

$X_I^b(k)$	$X_Q^b(k)$	$X_I^b(k+1)$	$X_Q^b(k+1)$
0	0	$\overline{\Delta x_I^b(k)}$	$\overline{\Delta x_Q^b(k)}$
0	1	$\overline{\Delta x_Q^b(k)}$	$\Delta x_I^b(k)$
1	1	$\Delta x_I^b(k)$	$\Delta x_Q^b(k)$
1	0	$\Delta x_Q^b(k)$	$\overline{\Delta x_I^b(k)}$

* Where $\overline{\Delta x_I^b(k)}$ is the negation of the $\Delta x_I^b(k)$

TABLE 2. RELATIONSHIP BETWEEN TRANSMITTED BITS AND CROSS-POLARIZATION DECISION BITS

$Y_I^b(k)$	$Y_Q^b(k)$	$X_I^b(k+1)$	$X_Q^b(k+1)$
0	0	$\overline{\Delta h_I^b(k)}$	$\overline{\Delta h_Q^b(k)}$
0	1	$\overline{\Delta h_Q^b(k)}$	Δh_I^b(k)
1	1	$\Delta h_I^b(k)$	$\Delta h_Q^b(k)$
1	0	$\Delta h_Q^b(k)$	$\overline{\Delta h_I^b(k)}$

III. SIMULATION RESULTS AND DISCUSSIONS

We performed simulations of the DSCD based PDM-DQPSK system to analyse the system performance. As shown in Fig. 6, the data bits are differentially coded at the transmitter, and chromatic dispersion is pre-compensated. The DAC and ADC are modeled using a 3rd order Bessel filter with a 3dB cutoff frequency of 45 GHz. The electrical signal from the DAC is modulated onto an optical carrier for transmission using an ideal IQ modulator. The modulated optical signal is transmitted to the receiver via a standard single-mode fiber (SMF). The received dual-polarized signal is differentially detected by the PDM-DQPSK receiver and then processed using DSP, including clock recovery (CLR), 4x4 MIMO adaptive equalization, carrier phase recovery (CPR), hard decision, CPEC, and BER calculation.

We also simulated an SHCD based PDM-QPSK system with the same parameters configuration, except that half the laser source power is used to transmit the remote LO. The simulation of SHCD system is simplified by considering for the remote LO only the power attenuation effect and ignoring other impairments. For fair comparisons, the OSNR of the SHCD system is calculated using the total transmitted optical power including both the signal and the remote LO.

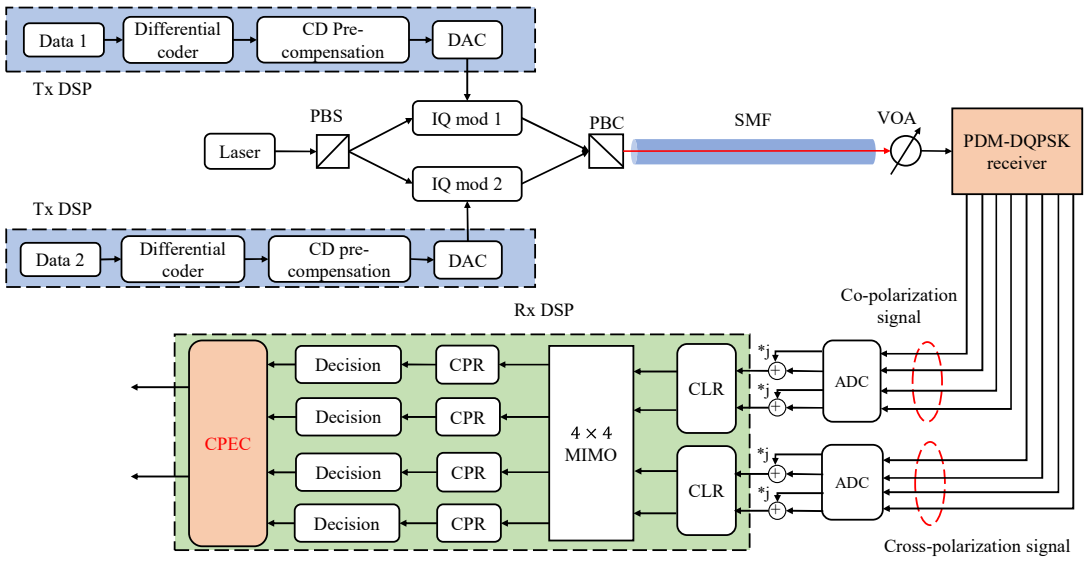

Fig. 6. Simulation setup for CPEC-enhanced differential self-coherent PDM-DQPSK system

As the laser linewidth is a key limiting factor for coherent detection solutions, including DSCD systems, coherent QPSK systems, and SHCD systems, comprehensive simulations are conducted to investigate the effect of the laser linewidth on these solutions. Fig. 7 demonstrates the laser linewidth tolerance of the conventional coherent detection, SHCD without path mismatch, and DSCD systems at different OSNR and at 200 Gb/s. The simulation results indicate that for laser linewidths above 1 MHz, BER of the conventional coherent detection system degrades to around 0.1, making it unusable. In contrast, the SHCD system without path mismatch and the DSCD system continue to work properly with above 1 MHz linewidth lasers. The DSCD system is less susceptible to phase noise as it uses the differential phase of two adjacent symbols for information transmission.

Fig. 8 further shows more stringent laser linewidth requirements of the SHCD system as the path mismatch length increases. At a path mismatch length of 0.5 m, BER of the SHCD system degrades to around 0.1 when the laser linewidth exceeds 7MHz. At a path mismatch length of 1 m, BER of the SHCD system degrades to around 0.1 when the laser linewidth exceeds 2MHz. On the other hand, the DSCD system can still operate normally with a 7 MHz laser. Therefore, the SHCD system requires extra DSP to improve its tolerance to path mismatch, whereas the DSCD scheme is intrinsically insensitive to the path mismatch problem.

The performance at 200 Gb/s of the DSCD based PDM-DQPSK without CPEC, CPEC-enhanced DSCD based PDM-DQPSK, SHCD based PDM-QPSK, and C-PDCR based PDM-QPSK systems are compared through 40 km SMF transmission simulations. As shown in Fig. 9, at 1×10^{-3}

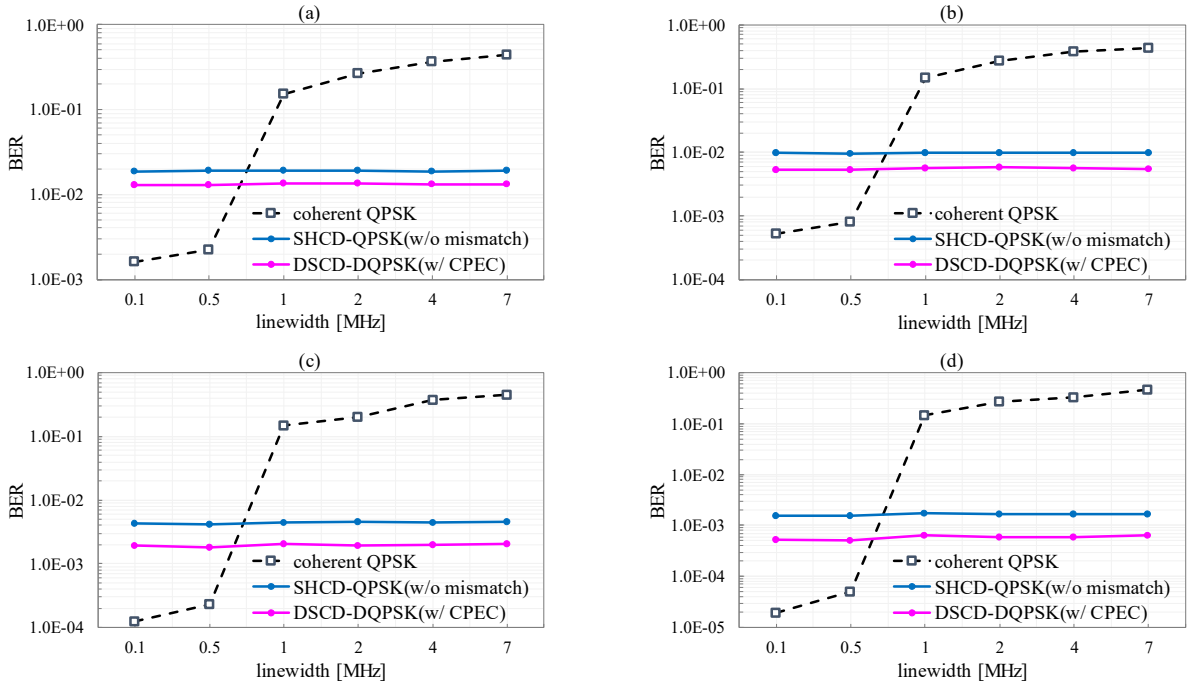

Fig.7. At 200 Gb/s, tolerance of conventional coherent PDM-QPSK system, SHCD based PDM-QPSK system without mismatch, and DSCD based PDM-DQPSK system for laser linewidth at different OSNR: (a) 16 dB OSNR, (b) 17 dB OSNR, (c) 18 dB OSNR, (d) 19 dB OSNR

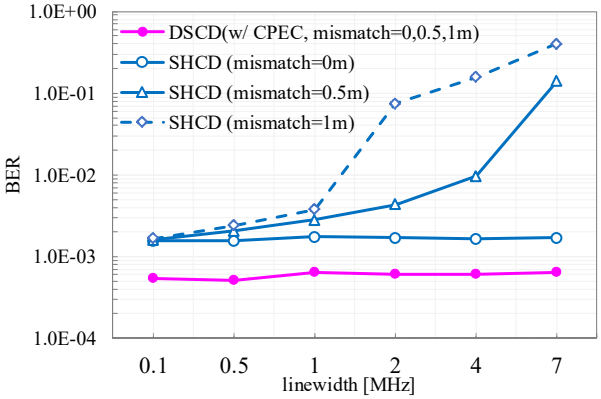

Fig. 8. Tolerance on laser linewidth of the SHCD and DSCD schemes with different path mismatches at 19 dB OSNR and 200 Gb/s bit rate

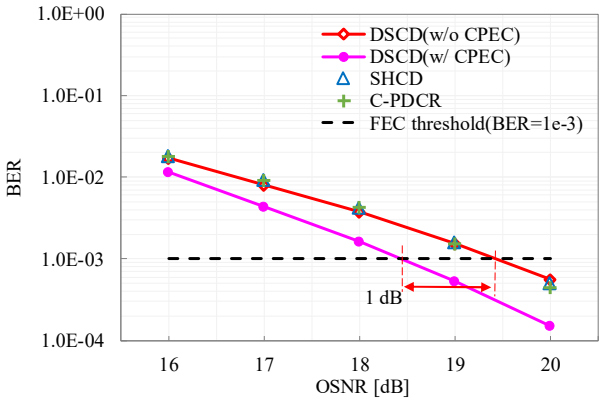

Fig. 9. OSNR requirement of DSCD, SHCD, and C-PDCR systems at 200Gb/s, where linewidth = 500kHz, mismatch = 0m

forward-error-correction (FEC) BER threshold, the required OSNR for DSCD without CPEC system is 19.4 dB, and the required OSNR for the CPEC-enhanced DSCD system is 18.4 dB. The results indicate that the proposed CPEC-enhanced DSCD system shows 1 dB advantage in OSNR sensitivity compared to the prior DSCD system [10].

In the SHCD system, the sum of signal power (P_s) and remote LO power (P_{LO}) is a fixed value, hence the value of the electrical power ($\sqrt{P_s \cdot P_{LO}}$) is maximized when $P_s = P_{LO}$. Therefore, the optimum LO-to-signal power ratio is 0.5 [6]. Fig. 9 also shows that, without path mismatch and with 500 kHz laser linewidth, the required OSNR at 1×10^{-3} BER of the simulated SHCD and C-PDCR systems are both 19.4 dB. It shows that compared to SHCD and C-PDCR systems, the CPEC-enhanced DSCD system achieves 1 dB improvement in receiver sensitivity. Besides, our system employs 4x4 adaptive equalization that enables digital domain polarization tracking, eliminating the need for complex and complicated optical polarization trackers. As expected, the implementation of the CPEC algorithm results in a notable enhancement of the DSCD system performance, which also leads to a significant improvement in receiver sensitivity.

IV. Summary

In this study, we proposed a CPEC-enhanced differential self-coherent PDM-DQPSK system as a solution for optical fiber transmission over short to medium distances. The proposed system facilitates implementation of fast polarization demultiplexing and tracking in digital domain. Moreover, the CPEC provides a novel error correction method that leverages cross-polarization terms for improved system performance. Compared to conventional coherent QPSK that requires receiver side LO, CPEC-enhanced differential self-coherent PDM-DQPSK system shows advantages in that it does not need receiver side LO, and shows higher laser linewidth tolerance. Furthermore, at 200 Gb/s bit rate and 1×10^{-3} FEC threshold, the simulation results showed that the proposed CPEC-enhanced DSCD system shows 1 dB advantage in OSNR sensitivity compared to the DSCD without CPEC, C-PDCR, and SHCD systems even for the case without fiber mismatch that degrades the SHCD system performance. Therefore, the proposed system is a promising solution for short-reach optical fiber transmissions.

References

[1] M. Chagnon, "Optical Communications for Short Reach," *Journal of Lightwave Technology,* vol. 37, no. 8, pp. 1779–1797, 2019.

[2] J. K. Perin, A. Shastri, and J. M. Kahn, "Design of Low-Power DSP-Free Coherent Receivers for Data Center Links," *Journal of Lightwave Technology,* vol. 35, no. 21, pp. 4650–4662, 2017.

[3] M. Morsy-Osman, M. Sowailem, E. El-Fiky, T. Goodwill, T. Hoang, S. Lessard, and D. V. Plant, "DSP-free 'coherent-lite' transceiver for next generation single wavelength optical intra-datacenter interconnects," *Opt Express,* vol. 26, no. 7, pp. 8890-8903, Apr 2 2018.

[4] M. Y. S. Sowailem, E. El-Fiky, M. Morsy-Osman, Q. Zhuge, T. M. Hoang, S. Paquet, C. Paquet, I. Woods, O. Liboiron-Ladouceur, and D. V. Plant, "Self-homodyne system for next generation intra-datacenter optical interconnects," *Opt Express,* vol. 25, no. 22, pp. 27834–27844, Oct 30 2017.

[5] Z. Feng, L. Xu, Q. Wu, M. Tang, S. Fu, W. Tong, P. P. Shum, and D. Liu, "Ultra-high capacity WDM-SDM optical access network with self-homodyne detection downstream and 32QAM-FBMC upstream," *Opt Express,* vol. 25, no. 6, pp. 5951–5961, Mar 20 2017.

[6] T. Gui, X. Wang, M. Tang, Y. Yu, Y. Lu, and L. Li, "Real-Time Demonstration of Homodyne Coherent Bidirectional Transmission for Next-Generation Data Center Interconnects," *Journal of Lightwave Technology,* vol. 39, no. 4, pp. 1231–1238, 2021.

[7] T. Gui, J. Cao, X. Chen, K. Zheng, S. Yuan, X. Fang, Y. Lei, Q. Zhan, D. Wang, and Q. Sui, "Real-time Single-Carrier 800Gb/s DP-64QAM Demonstration using Bi-Directional Self-homodyne Coherent Transceivers with 200krad/s Endless Active Polarization Controller," in *Optoelectronics and Communications Conference*, 2021: Optical Society of America, p. T5A. 5.

[8] H. Ji, J. Li, X. Li, S. Dong, Z. Xu, Y. Su, and W. Shieh, "Beyond Mrad/s Polarization Tracking Speed of Complementary Polarization-diversity Coherent Receiver for Remote LO," in *2022 Optical Fiber Communications Conference and Exhibition (OFC)*, 2022: IEEE, pp. 1-3.

[9] H. Ji, J. Li, X. Li, S. Dong, Z. Xu, Y. Su, and W. Shieh, "Complementary Polarization-diversity Self-Coherent Homodyne Receiver with Rapid Polarization Tracking for Remote LO," in *2022 Optical Fiber Communications Conference and Exhibition (OFC)*, 2022: IEEE, pp. 1–3.

[10] R. Nagarajan, J. Rahn, M. Kato, J. Pleumeekers, D. Lambert, V. Lal, H.-S. Tsai, A. Nilsson, A. Dentai, M. Kuntz, R. Malendevich, J. Tang, J. Zhang, T. Butrie, M. Raburn, B. Little, W. Chen, G. Goldfarb, V. Dominic, B. Taylor, M. Reffle, F. Kish, and D. Welch, "10 Channel, 45.6 Gb/s per Channel, Polarization-Multiplexed DQPSK, InP Receiver Photonic Integrated Circuit," *Journal of Lightwave Technology,* vol. 29, no. 4, pp. 386–395, 2011.